# AREVA Calculation No. 32-9221080-000

# Diablo Canyon Unit 2 Pressurizer Safety/Relief Nozzles Laminar/Planar Flaw Analysis – Non Proprietary

AREVA

# CALCULATION SUMMARY SHEET (CSS)

Document No. 32 - 9221080 - 000 Safety Related: ☒ Yes ☐ No

Title Diablo Canyon Unit 2 Pressurizer Safety/Relief Nozzles Laminar/Planar Flaw Analysis – Non Proprietary

PURPOSE AND SUMMARY OF RESULTS:

Purpose

An inservice inspection of Diablo Canyon Power Plant (DCPP) Unit 2 overlaid Pressurizer (PZR) Safety nozzles revealed the existence of indications. The indications are described in the Diablo Canyon Power Plant Design Input Transmittal (DIT) summarized in Reference [1]. Previous disposition of all reported laminar and planar indications per the rules of the acceptance standards Table IWB-3514-3 of ASME B&PV Code Section XI [2] and Section III [3] are documented in References [4] and [5]. The purpose of this document is to validate that the acceptance standards under IWB-3500 remain valid after any potential crack growth.

This document analyzes the indications for the remaining 38 years of plant operation. The indications are all embedded within the body of the weld overlay and nozzle. Therefore, no primary water stress corrosion crack growth would occur. The only mechanism by which indications could grow is fatigue crack growth. In this document crack growth of postulated flaws and evaluation of the final flaw sizes in accordance with the rules of ASME B&PV Code Section XI [2] and Section III [3] are performed. Reference [6] Section 4.6, item 3 states that the applicable ASME Code year is 2004 with addenda through 2005.

This document is the Non-Proprietary document of 32-9215965-001.

Summary of Results

The final crack sizes for all laminar flaw cases are summarized in Table 7-5. The flaw area evaluation and overlay length evaluation are performed in Table 7-6 and Table 7-7, respectively. The final flaw size of the planar flaw is shown in Table 7-8 and the flaw evaluation is summarized in Table 7-10. It is concluded that all laminar and planar flaws meet the acceptance criteria of Section XI the ASME Code [2] for the 38 years of plant operation.

THE FOLLOWING COMPUTER CODES HAVE BEEN USED IN THIS DOCUMENT:

| CODE/VERSION/REV | CODE/VERSION/REV |
|---|---|
| AREVACGC 5.0 / (Windows 7) | |
| | |

THE DOCUMENT CONTAINS ASSUMPTIONS THAT SHALL BE VERIFIED PRIOR TO USE

☐ YES
☒ NO

AREVA

0402-01-F01 (Rev. 018, 01/31/2014)
Document No. 32-9221080-000

Diablo Canyon Unit 2 Pressurizer Safety/Relief Nozzles Laminar/Planar Flaw Analysis – Non Proprietary

Review Method: ☒ Design Review (Detailed Check)
☐ Alternate Calculation

## Signature Block

| Name and Title (printed or typed) | Signature | P/R/A and LP/LR | Date | Pages/Sections Prepared/Reviewed/Approved |
|---|---|---|---|---|
| Silvester J. Noronha<br>Principal Engineer | SJNoronha | P | 3/28/14 | All |
| Samer H. Mahmoud<br>Principal Engineer | SHM | R | 3-28-14 | All |
| Tim M. Wiger<br>Manager I | T.M. Wiger | A | 3/28/14 | All |
| | | | | |

Note: P/R/A designates Preparer (P), Reviewer (R), Approver (A);
LP/LR designates Lead Preparer (LP), Lead Reviewer (LR)

### Project Manager Approval of Customer References (N/A if not applicable)

| Name (printed or typed) | Title (printed or typed) | Signature | Date |
|---|---|---|---|
| N/A | N/A | N/A | N/A |

### Mentoring Information (not required per 0402-01)

| Name (printed or typed) | Title (printed or typed) | Mentor to: (P/R) | Signature | Date |
|---|---|---|---|---|
| N/A | N/A | N/A | N/A | N/A |
| | | | | |

## Record of Revision

| Revision No. | Pages/Sections/Paragraphs Changed | Brief Description / Change Authorization |
|---|---|---|
| 000 | All | Original Release |
| | | |
| | | |
| | | |
| | | |
| | | |
| | | |
| | | |
| | | |
| | | |
| | | |
| | | |
| | | |
| | | |

## Table of Contents

Page

## Table of Contents
(continued)

## List of Tables

## List of Figures

## 1.0 INTRODUCTION

An inservice inspection of Diablo Canyon Power Plant (DCPP) Unit 2 overlaid Pressurizer (PZR) Safety nozzles revealed the existence of indications. The indications are described in the Diablo Canyon Power Plant Design Input Transmittal (DIT) documented in Reference [1]. Previous dispositions of all reported indications per the rules of the acceptance standards Table IWB-3514-3 and Article NB-3227.2 of ASME B&PV Code Section XI [2] and Section III [3] respectively are documented in References [4] and [5].The purpose of this document is to validate that the acceptance standards under IWB-3500 remain valid after any potential crack growth.

Indications observed in the PZR Safety nozzles are primarily laminar, with the exception of an indication located near the shoulder of Nozzle Safety A. This document analyzes the indications for 38 years of remaining plant life. The indications are all embedded within the body of the nozzle and overlay. Therefore, no primary water stress corrosion crack growth mechanism would occur. The only mechanism by which indications could grow is fatigue crack growth.

This document provides a description of the indications, postulated flaws, applicable fatigue crack growth laws, fatigue crack growth analysis, and finally the predicted final flaw sizes are evaluated in accordance with the rules of ASME B&PV Code Section XI [2] and Section III [3]. The applicable ASME code year for this analysis is 2004 with addenda through 2005 [6].

## 2.0 ANALYTICAL METHODOLOGY

This document performs flaw evaluation for dispositioning the non-destructive examination (NDE) found indication in the DCPP PZR Safety nozzles. As described in Reference [1], all indications were laminar in nature with the exception of the indication found near the shoulder of PZR Safety nozzle A, which had small planar dimension. This document postulates cylindrical flaws to analyze the laminar indication. For the planar extent of the indication located near the PZR Safety nozzle A shoulder, a subsurface circumferential planar flaw was postulated.

For each postulated flaw, the flaw evaluation methodology consists of performing fatigue flaw growth for the specified service life. At the end of life, a flaw evaluation is performed to evaluate the end of life flaw acceptability.

This analysis postulated laminar cylindrical and planar circumferential sub-surface flaws which could propagate by fatigue crack growth through the full structural weld overlay (FSWOL) and/or the Safety nozzle. A linear elastic fracture mechanics (LEFM) analysis was performed to determine the applied stress intensity factors (SIFs) for the laminar and planar flaw indications. The center-cracked panel (CCP) model was used with the radial and shear stresses to compute stress intensity factors for the laminar flaw indications. Flaw growth in the axial direction to estimate final flaw width was calculated using the SIF from the CCP model. Circumferential crack growth for estimating the final flaw length was evaluated by extending the flaw length in proportion to the ratio of final flaw width to the initial flaw width. Planar flaws were modelled as 360° circumferential flaws.

It should be noted that the prior planar flaw analysis for DCPP Unit 2 PZR nozzles [5] used 38 years of remaining service life. The current analysis was performed using the 38 years of remaining service life as well. The crack growth analysis considered the growth of embedded flaws due to cyclic loadings under the presence of residual stress from the welding processes. The final flaw sizes were calculated using the same operating transients considered in the original 2007 flaw growth analysis [7]. The predicted final flaw sizes were evaluated in accordance with the rules of ASME B&PV Code Section XI Table IWB-3514-3 [2] for laminar flaws. For planar flaws, the predicted final flaw sizes were evaluated in accordance with the rules of ASME B&PV Code Section XI IWB-3612 and IWB-3640 [2]. Section III article NB-3227.2 [3], was used to verify that the weld overlay length excluding the indications is sufficient to transfer the load through shear back to the base metal considering a 100% through wall crack in the PWSCC susceptible material.

The initial structural overlay analysis was performed in 2007 per ASME Section III Subsection NB Code with 2001 through 2003 Addenda. During relief request of 2013, the shear stress check for the laminar flaw analysis was performed per ASME Section III Subsection NB Code with 2004 and 2005 Addenda. The review was performed for both Code years and it was determined the criteria for pure shear stress evaluation per NB-3227.2 are the same. Hence, it is concluded that both the Codes are applicable to the current analyses and no additional reconciliation is required.

The following subsections describe the analytical methodology used in analyzing both the laminar and the planar indications. Also, a list of the abbreviations and parameters used thought the document is provided.

## 2.1 Laminar Flaw Analysis

This section outlines the analytical methodology used to analyze the laminar indications. The laminar flaw analytical procedure include, the models used to calculate the stress intensity factors (SIF) for laminar flaws, laminar flaw crack growth calculation procedure, laminar flaw evaluation, and FSWOL minimum length requirement evaluation.

### 2.1.1 Laminar Flaw Stress Intensity Factor Solutions

To calculate the stress intensity factor for the laminar flaw, the closed-form SIF solutions from page 40 of Reference [8] for CCP model were used. The Mode I and Mode II configurations are illustrated in Figure 2-1.

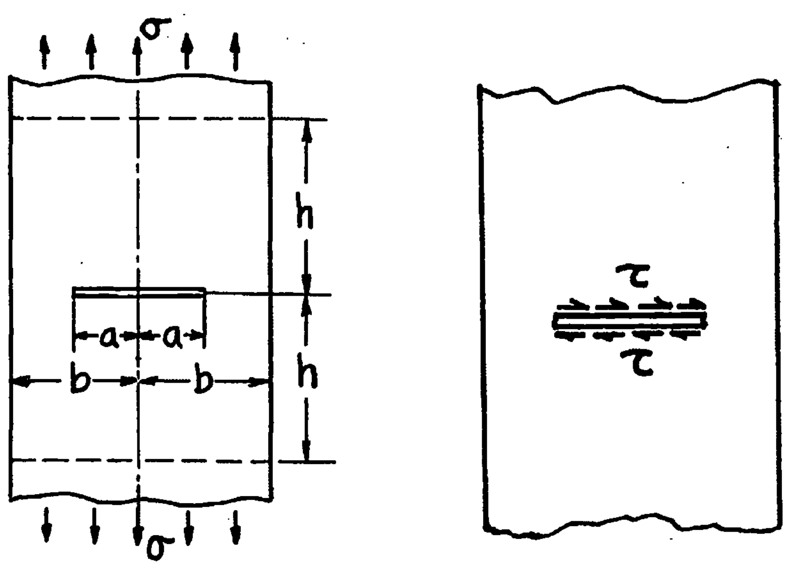


(Mode I) (Mode II)

**Figure 2-1: A Through-Wall Crack in the Center of a Plate**

For Mode I configuration, the $K_I$ solution is listed below:

$$K_I = \sigma\sqrt{\pi a} \cdot F\left(a/b\right)$$

$$F\left(a/b\right) = \left[1 - 0.025\left(a/b\right)^2 + 0.06\left(a/b\right)^4\right]\sqrt{\sec\frac{\pi a}{2b}}$$

Where, $\sigma$ = uniform tensile stress

2a = crack width

2b = plate width

For Mode II configuration, the $K_{II}$ solution is identical to that in Mode I except using $\tau$ (uniform shear stress) instead of $\sigma$ (uniform tensile stress). It should be noted that some geometry idealization was made to use the CCP model SIF solution to analyze the Safety Nozzle laminar indications.

The functions F(a/b) is a geometry correction factor in which the b parameter accounts for the free surface effects. For an a/b value of 0, F(0)=1 and for an a/b value of 1, the geometry correction factor F(a/b) asymptotically approaches a very large value. For an a/b value of 99.9%, F(0.999) = 26.1. The selection of the b parameter should be based on the location of the closest free boundary to the analyzed flaw. Considering the Safety nozzle geometry, the b parameter can be quite large.

### 2.1.2 Laminar Flaw Fatigue Crack Growth Calculation

The steps to perform fatigue crack growth calculation for laminar flaws are presented below. Note that the analysis assumed 360° laminar flaw, which is very conservative. Since the full circumference was assumed cracked; this section evaluated fatigue crack growth in the axial direction only.

1. For the first transient, Calculate the mode I maximum and minimum stress intensity factors ($K_{Imax}$ and $K_{Imin}$) based on the maximum radial stress $\sigma_{x\_max}$ and minimum radial stress $\sigma_{x\_min}$ in the first transient, respectively. Crack length 2*a* (crack width) and 2*b* (plate width) are also required to calculate the SIF.
2. Calculate the stress intensity factor range due the radial stress ($\Delta K_I = K_{Imax} - K_{Imin}$).
3. Calculate the mode II maximum and minimum stress intensity factors ($K_{IImax}$ and $K_{IImin}$) based on the maximum shear stress $\tau_{max}$ and minimum shear stress $\tau_{min}$ in the first transient, respectively. Crack width (2*a*) and plate width (2*b*) are also required to calculate the SIF.
4. Calculate the stress intensity factor range due the shear stress ($\Delta K_{II} = K_{IImax} - K_{IImin}$).
5. Combine the stress intensity factor ranges from steps 2 and 4 to calculate the effective stress intensity factor range ($\Delta K$) to be used in the crack growth analysis as $\Delta K = [(\Delta K_I)^2 + (\Delta K_{II})^2]^{0.5}$.
6. To account for mean stress effect, calculate an effective R ratio as $R = 1 - \Delta K / K_{max}$ using $K_{max} = [(K_{Imax})^2 + (K_{IImax})^2]^{0.5}$ and $\Delta K = [(\Delta K_I)^2 + (\Delta K_{II})^2]^{0.5}$. The R ratio is used in the crack growth equations to account for mean stress effect as described in Section 4.7.

7. Calculate crack growth increment ($2\Delta a$) based on $\Delta K$, R, and number of cycles per year for the specific transient. Metal temperature is also required to determine the parameters in the crack growth rate equation.
8. Update crack length to find the crack length at the end of the transient ($2a_f = 2a_i + 2\Delta a$), where $2a_f$ is the crack length at the end of the transient, $2a_i$ is the crack length at the beginning of the transient, and $2\Delta a$ is the crack growth increment during the transient as calculated in Step 7.
9. Repeat steps 1 through 8 for transients 2 through 10 with the crack length at the end of transient 1 is used as the starting crack length for transient 2, the crack length at the end of transient 2 is used as the starting crack length for transient 3 and so on. The crack length at the end of the last transient is also the crack length at the end of one year.
10. Repeat steps 1 through 9 to find crack length at the end of subsequent years with the crack length at the end of the first year is used as the starting crack length for the second year, the crack length at the end of the second year is used as the starting crack length for the third year and so on. The process is repeated for the subsequent years for the 38 year design life.

### 2.1.3 Laminar Flaw Evaluation

Disposition of all reported laminar indications per the rules of the acceptance standards in Table IWB-3514-3 of ASME B&PV Code Section XI [2] are reported in Reference [4]. The same evaluation procedure was used in this document with final crack length now updated with calculated crack growth for 38 years of plant operation. For indication area evaluation, the acceptance criterion is in Table IWB-3514-3 [2], which requires that

$$A = 0.75(w \times l) \leq 7.5\ in^2$$

where $A$ is the flaw area, $w$ and $l$ are flaw width and length.

### 2.1.4 Minimum Required Overlay Length Calculations

For overlay length evaluation, the length of the weld overlay is acceptable provided that the effective overlay length ($l_{eff}$) is greater than the required overlay length ($l_{req}$). The required overlay length ($l_{req}$) is the length of the weld overlay that is sufficient to transfer the load through shear back to the base metal. Conservatively a 100% through wall crack is considered in the PWSCC (primary water stress corrosion cracking) susceptible material. The formulation in this section provides the procedure used for evaluating the minimum overlay length requirement.

The cross-sectional area ($A_{net}$) and section modulus ($Z_{net}$) of the net section are calculated considering a 100% through wall crack in the PWSCC susceptible material as

$$A_{net} = \frac{\pi}{4}\left((D+2t)^2 - D^2\right)$$

$$Z_{net} = \frac{2 \times I_{net}}{(D+2t)} = \frac{2 \times \frac{\pi}{64}((D+2t)^4 - D^4)}{(D+2t)}$$

where $D$ is the OD of the nozzle base metal, and $t$ is the minimum weld overlay thickness.

The extreme fiber tensile stress is calculated based on the net section properties with faulted moment (*M*) and axial load (*F*).

$$\sigma_{net} = \frac{M}{Z_{net}} + \frac{F}{A_{net}}$$

Conservatively consider the maximum allowable shear stress for the faulted case to be 0.6Sm (see NB-3227.2, Reference [5]) although the faulted allowable shear stress is higher. A force balance on the FSWOL with the maximum shear stress at the interface gives

$$\sigma_{net} \times t = 0.6 S_m \, l_{req}$$

Solving for the required minimum overlay length, $l_{req}$, gives

$$l_{req} = \frac{\sigma_{net} \times t}{0.6 S_m}$$

The effective length, $l_{eff}$, of the weld overlay is

$$l_{eff} = l_{wol} - l_{flaw}$$

where $l_{wol}$ is the length of the weld overlay based on the design drawings for minimum thickness conditions and $l_{flaw}$ is the axial dimension of the laminar flaw. Thus the length of the weld overlay is acceptable provided that $l_{eff}$ is greater than $l_{req}$.

It is noted that the initial structural overlay analysis was performed in 2007 per ASME Section III Subsection NB Code with 2001 and 2003 Addenda. During relief request of 2013, the shear stress check for the laminar flaw analysis was performed per ASME Section III Subsection NB Code with 2004 and 2005 Addenda. Both Code years were reviewed and it was determined that the criteria for pure shear stress evaluation per NB-3227.2 are the same. Hence, it is concluded that both Codes are applicable to the current analyses and no additional reconciliation is required.

## 2.2 Planar Flaw Analysis

This section outlines the analytical methodology used to analyze the planar indications. The planar flaw analytical procedure include, the models used to calculate the stress intensity factors (SIF) for planar flaws, planar flaw crack growth calculation procedure, and planar flaw evaluation.

### 2.2.1 Planar Circumferential Flaw

The planar projection of the PZR safety nozzle A indications is shown in Figure 2-2. The corresponding idealized flaw shape for fracture mechanics evaluation is shown in Figure 2-3. The flaw was assumed to be full 360° circumferential flaw that is embedded entirely in the FSWOL with one flaw tip located at the interface of the nozzle and the FSWOL and the other flaw tip extending 0.08 inch into the FSWOL.

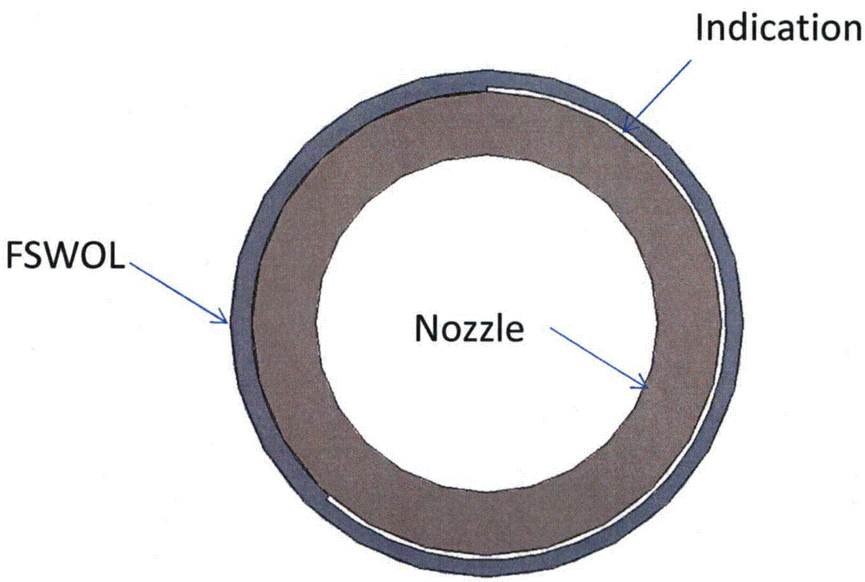


**Figure 2-2: Planar Projection of PZR Safety Nozzle A Indication**

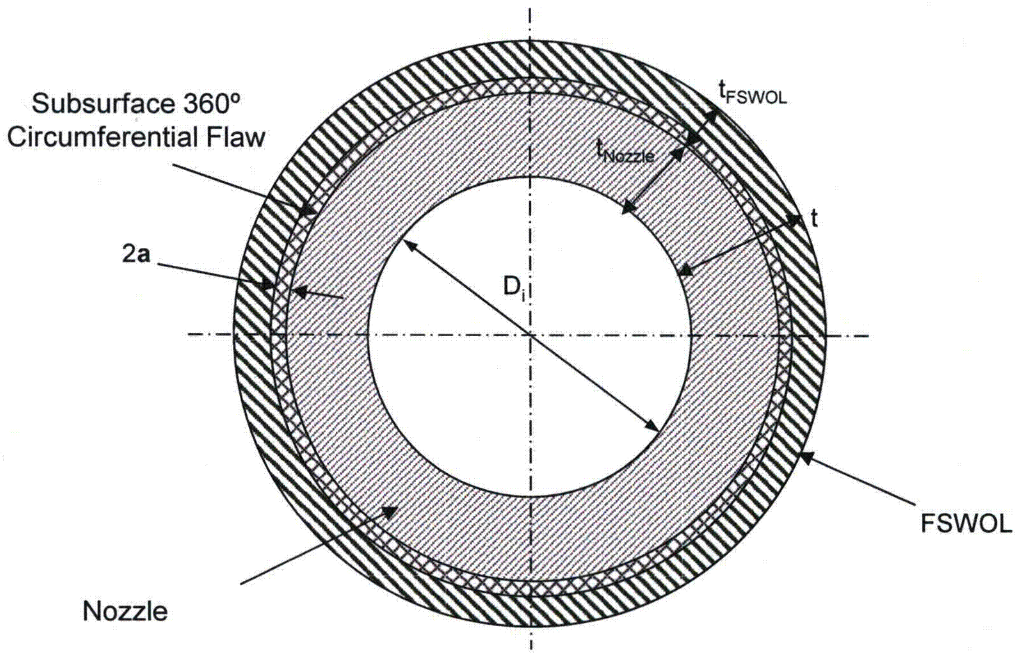


**Figure 2-3: PZR Safety Nozzle A Idealized Indication**

### 2.2.2 Flaw Growth Analysis - Planar Flaw

AREVACGC [9] was used to perform fatigue crack growth for the postulated planar flaw near the shoulder of PZR Safety Nozzle A. AREVACGC [9] uses the weight function method for calculating the stress intensity factor (SIF), which is documented in Reference [10]. AREVACGC computes the SIF internally and perform the fatigue crack growth calculations to estimate the final flaw size at the end of the service life. Necessary inputs to AREVACGC include nozzle geometry, flaw shape, size, orientation, applied stress, transient cycles, and temperature. The fatigue crack growth rates for the materials of interest (Low Alloy Steel nozzle and Alloy 52 FSWOL), implemented in AREVACGC, can be activated by choosing appropriate input flags. The Low Alloy Steel fatigue crack growth rates are obtained from A-4300 of Reference [2] and the Alloy 52/52M fatigue crack growth rates are obtained from Reference [15].

For the postulated subsurface circumferential planar flaw, the applied stress intensity factor is driven by the axial stresses. The relevant sources of axial stress for fatigue crack growth analyses of the postulated circumferential (planar) flaw are attributed to the occasional stresses from the operating transients, and sustained stresses due to weld residuals and pipe loads (Deadweight and Thermal Expansion). The operating transient stresses are due to through-wall thermal gradients and pressure fluctuations during the transients. For startup/shutdown (HUCD), the thermal expansion pipe loads are applied cyclically to account for the change in thermal expansion load between cold shutdown and operating conditions.

Flaw growth is calculated in one-year increments. As stated earlier a service life of 38 years was used in the current analysis. The highest metal temperature during a transient was used to determine the fatigue crack growth rates.

### 2.2.3 Planar Flaw Evaluation

Because the planar flaw is located on the interface of the weld overlay and the nozzle with one crack tip located in the overlay and the other crack tip is near the overlay/nozzle interface, the predicted final flaw size was evaluated in accordance with the rules of ASME B&PV Code Section XI IWB-3612 and IWB-3640 [2].

Per the ASME B&PV Code Section XI IWB-3612 evaluation procedure, a flaw is acceptable if the applied stress intensity factor and the flaw size satisfy the following conditions

(a) For Normal and Upset conditions (Service Levels A and B)

$$K_I < K_{Ia} \sqrt{10}$$

(b) For Emergency and Faulted conditions (Service Levels C and D)

$$K_I < K_{IC} \sqrt{2}$$

Where

$K_I$ = the maximum applied stress intensity factor

$K_{Ia}$ = the available fracture toughness based on crack arrest for the corresponding crack tip temperature

$K_{IC}$ = the available fracture toughness based on crack initiation for the corresponding crack tip temperature

The analytical procedure for evaluating the rules of IWB-3640 is outlined in Appendix C of ASME B&PV Code Section XI [2]. The appropriate evaluation procedure for the postulated subsurface circumferential planar flaw is given in article C-5000 [2], which deals with ductile materials where the failure mode is that of plastic collapse at limit load.

Per Reference [2] the limiting load combinations for primary bending stress ($\sigma_b$) for the ASME B&PV Code Section XI Service Level conditions are as follows:

| | |
|---|---|
| Service Level A (Normal) - | DW |
| Service Level B (Upset) - | DW + OBE |
| Service Level C (Emergency) - | No Transient or Load specified for this condition |
| Service Level D (Faulted) - | DW + DDE + HOSGRI (conservatively summed) |

### 2.3 List of Abbreviation and Parameters

This section defines the various abbreviations and parameters used throughout the document.

***Abbreviations***

| | |
|---|---|
| *DCPP* | Diablo Canyon Power Plant |
| *PZR* | Pressurizer |
| *DIT* | Design Input Transmittal |
| *PWSCC* | Primary Water Stress Corrosion Crack |
| *NDE* | Non-Destructive Examination |
| *FSWOL* | Full Structural Weld Overlay |
| *LEFM* | Linear Elastic Fracture Mechanics |
| *CCP* | Center-Cracked Panel Model |
| *SIF* | Stress intensity factor |
| *DE* | Design Earthquake |
| *DDE* | Double Design Earthquake |
| *OBE* | Operation Basis Earthquake |

***Parameters for crack growth analysis***

| | | |
|---|---|---|
| $2a$ | Flaw width (in the axial direction) used in the CCP model SIF calculations | (in) |
| $2b$ | Plate width parameter used in the CCP model SIF calculations | (in) |
| $K_I$ | Mode I stress intensity factor | (ksi√in / MPa√m) |
| $K_{II}$ | Mode II stress intensity factor | (ksi√in / MPa√m) |
| $\Delta K_I = K_{Imax} - K_{Imin}$ | Mode I stress intensity factor range | (ksi√in / MPa√m) |
| $\Delta K_{II} = K_{IImax} - K_{IImin}$ | Mode II stress intensity factor range | (ksi√in / MPa√m) |
| $\Delta K = [(\Delta K_I)^2 + (\Delta K_{II})^2]^{0.5}$ | Mixed mode stress intensity factor range | (ksi√in / MPa√m) |
| $K_{max} = [(K_{Imax})^2 + (K_{IImax})^2]^{0.5}$ | Mixed mode maximum stress intensity factor | (ksi√in / MPa√m) |
| $R = 1 - \Delta K / K_{max}$ | Mixed mode R ratio | |
| $\sigma_{op\ max}$ | Maximum operating radial stress | (psi) |
| $\sigma_{op\ min}$ | Minimum operating radial stress | (psi) |
| $\tau_{op\ max}$ | Maximum operating shear stress | (psi) |
| $\tau_{op\ min}$ | Minimum operating shear stress | (psi) |

| | | |
|---|---|---|
| $\sigma_{x\ max}$ | Maximum radial stress | (psi) |
| $\sigma_{x\ min}$ | Minimum radial stress | (psi) |
| $\sigma_{rs}$ | Residual radial stress | (psi) |
| $\tau_{rs}$ | Residual shear stress | (psi) |
| $\sigma_{max}$ | Maximum radial stress | (psi) |
| $\sigma_{min}$ | Minimum radial stress | (psi) |
| $\tau_{max}$ | Maximum shear stress | (psi) |
| $\tau_{min}$ | Minimum shear stress | (psi) |
| $2a_i$ | Initial flaw width | (in) |
| $2a_f$ | Final flaw width | (in) |
| $2\Delta a$ | Flaw growth increment | (in) |
| $\Delta N$ | Number of cycles per year for a given transient in one direction | (cycle/year) |

**Parameters used in indication area evaluation**

| | | |
|---|---|---|
| $A$ | Laminar indication area | ($in^2$) |
| $w$ | Flaw width used in the indication area evaluation | (in) |
| $l$ | Flaw length used in the indication area evaluation | (in) |

**Parameters for crack growth rate equations**

| | | |
|---|---|---|
| $da/dN$ | Crack growth rate | (in/cycle) |
| $n$ | Crack growth equation exponent | |
| $T$ | Temperature | (°F or °C) |
| $C_{A600}, C, Co, S, S_R$ | Coefficients in the crack growth equations | |
| $R$ | R ratio | |

**Parameters for required overlay length evaluation**

| | | |
|---|---|---|
| $A_{net}$ | Cross-sectional area of the weld overlay | ($in^2$) |
| $Z_{net}$ | Section modulus of the weld overlay | ($in^3$) |
| $\sigma_{net}$ | Tensile stress is calculated based on the net section properties with faulted moment | (psi) |
| $l_{req}$ | Required overlay length to transfer the load through shear back to the base metal | (in) |
| $l_{eff}$ | Effective length of the weld overlay | (in) |
| $l_{wol}$ | Length of the weld overlay based on the design drawing | (in) |
| $l_{flaw}$ | Axial dimension of the laminar flaw used in required overlay length assessment | (in) |
| $OD$ | Outer diameter | (in) |
| $D$ | Diameter (same as outer diameter) | (in) |
| $t$ | Thickness (weld overlay) | (in) |
| $F$ | Axial load | (lbf) |
| $M$ | Bending Moment | (in-lbf) |

## 3.0 ASSUMPTIONS

This section discusses the assumptions and modeling simplifications used in this evaluation of Diablo Canyon Unit 2 PZR Safety Nozzles indications.

### 3.1 Unverified Assumptions

There are no assumptions that must be verified before the present analysis can be used to support the disposition of the Diablo Canyon Unit 2 PZR Safety Nozzles indications.

### 3.2 Justified Assumptions

1. For the case where the R ratio < 0 (or similarly $K_{min} < 0$), the R ratio is set equal to zero and the full range of $\Delta K$ is used in the crack growth calculations. This is a conservative assumption since crack closure due to compressive stress field is ignored.
2. The analysis assumed 360° laminar and planar flaws for fatigue crack growth calculations, which are conservative assumptions.
3. For laminar flaws, fatigue crack growth was performed in the axial (width) direction. Final circumferential flaw length was estimated by extending the initial flaw length proportional to the ratio of the final flaw width to initial flaw width. This is a conservative assumption since flaw growth in the circumferential (length) direction is expected to be less than the flaw growth in the axial (width) direction.

### 3.3 Modeling Simplifications

1. Multiple laminar flaws in Reference [1] are combined into larger, bounding flaws and extended to include a complete 360° arc length for crack growth calculations. Conservatively, CCP model is used to represent the 360° laminar flaws.
2. For laminar flaw evaluation, the mode I and mode II were combined using the Square Root of Sum of Squares (SRSS) of the respective stress intensity factors. This results in a more conservative crack growth estimation than that obtained by the linear summation of the individual crack growth increments due to mode I and mode II when the crack growth law exponent is equal to or greater than 2 (i.e. for crack growth law proportional to $\Delta K^n$, when n is equal to or greater than 2, combining mode I and Mode II using the SRSS method results in a conservative estimation of the crack growth increment).
3. The 2b parameter for analyzing the laminar indications was defined as either the distance between the point where the overlay meets the nozzle and the butter or distance to the nearest free surface.

### 3.4 Engineering Judgment

Contribution of the external loads to the fatigue crack growth of the laminar flaws analyzed in the current document was assumed to be negligible. This is an engineering judgment since the sustained external loads will have minimal contributions to the cyclical radial and shear stress components.

## 4.0 DESIGN INPUTS

### 4.1 Geometry

Figure 4-1 shows a schematic view of the PZR Safety nozzle with FSWOL (taken from Reference [12]). The different parts/subcomponents of the PZR Safety nozzle are labeled in Figure 4-1.

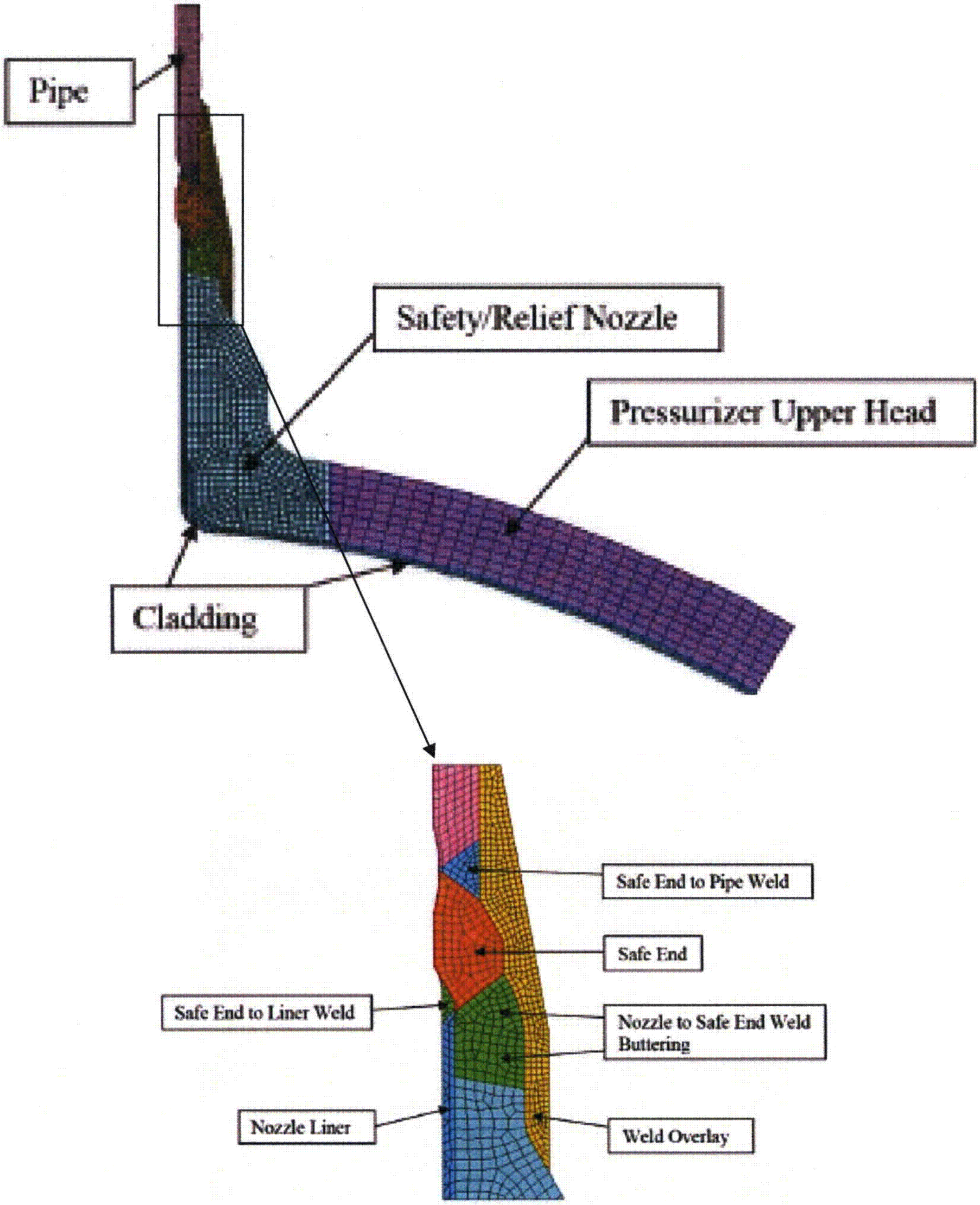


**Figure 4-1: Schematic of Safety/Relief Nozzle with FSWOL**

The indications detected in the PZR Safety nozzle A are shown on Figure 4-2 and Figure 4-3 with additional information provided in the Indication Data Sheets "*Safety Nozzle "A" WIB-369 OL*" in Reference [1]. Figure 4-4 and Figure 4-5 show indications detected in Nozzle B with further information in "*Safety Nozzle "B" WIB-423 OL*". The indications detected in Nozzle C are shown in Figure 4-6 and Figure 4-7, the corresponding additional are given in "*Safety Nozzle "C" WIB-359 OL*" (Reference [1]). Detailed dimensions of the safety nozzles are in Reference [11].

[ ]

**Figure 4-2: WIB-369 Overlay Rollout "A" Safety Nozzle (Ref. [1])**

[ ]

**Figure 4-3: Safety Nozzle "A" WIB-369 Overlay Indication Plot (Ref. [1])**

[ ]

**Figure 4-4: WIB-423 Overlay Rollout "B" Safety Nozzle (Ref. [1])**

[ ]

**Figure 4-5: Safety Nozzle "B" WIB-423 Overlay Indication Plot (Ref. [1])**

**Figure 4-6: WIB-359 Overlay Rollout "C" Safety Nozzle (Ref. [1])**

**Figure 4-7: Safety Nozzle "C" WIB-359 Overlay Indication Plot (Ref. [1])**

To enable conservative 2D axisymmetric analysis of laminar flaws, the circumferential content of the laminar flaws are combined and extended to include a complete 360° arc length. The longitudinal (axial) content of the laminar flaws are combined according to the ASME Code Section XI proximity rules. Therefore, it is determined in Reference [12] that the indications in Safety Nozzle B are combined as one bounding flaw along FLB, as shown in Figure 4-8. Indication #3 in Nozzle C is covered by the bounding flaw analysis along FLA of indications #1/1A of Nozzle A.

Since the indications in Figure 4-3 and Figure 4-5 are located at the interfaces of two different materials, two cases for each indication were analyzed. In one case, flaw growth rates of the Alloy 52/52M (WOL) were used and in the other case flaw growth rates of Low Alloy Steel (Nozzle) were used. Reference [12] defines path line cases, FLA_wol and FLA_noz, whose locations are identical to FLA, the stresses for FLA_wol were extracted by selecting WOL material only and the stresses for FLA_noz were extracted by selecting nozzle material only. All path lines are shown in Figure 4-8. For path line FLB the path line cases FLB_wol and FLB_noz are defined by selecting WOL material and nozzle material, respectively as shown in Figure 4-8. Since the laminar indication #4 in Nozzle C is entirely within the WOL, only FLC2_wol is required for the analysis. Thus fatigue crack growths for these five laminar flaw cases were analyzed. Planar indications were only detected in Nozzle A and hence only path line FLA_pln is used in the analysis. The path lines shown in parentheses in Figure 4-8 are for information only and are not considered in the analysis.

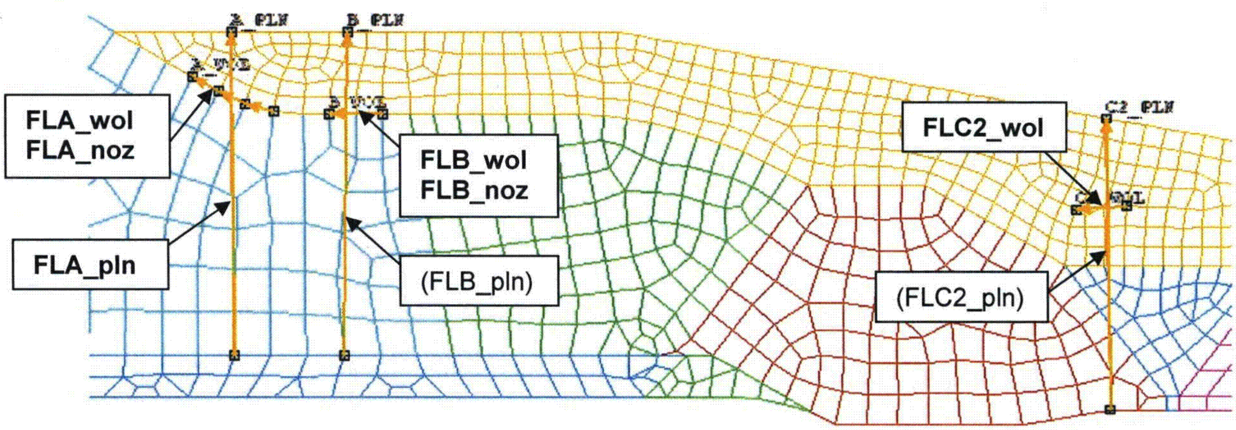


**Figure 4-8: PZR Safety Nozzle with Path Lines Superposed**

For the five laminar path line cases analyzed in this document, the crack dimensions required for calculating the SIF are listed in Table 4-1.

**Table 4-1: Dimensions of laminar flaws for SIF Calculation**

| Path Line Case | 2a [(1)] (inch) | 2b (inch) |
|---|---|---|
| FLA_wol | [ ] | [ ] |
| FLA_noz | [ ] | [ ] |
| FLB_wol | [ ] | [ ] |
| FLB_noz | [ ] | [ ] |
| FLC2_wol | [ ] | [ ] |

Note [(1)]: Flaw indication lengths are obtained from Reference [1].
[(2)]: From Reference [4]
[(3)]: From Reference [1] and [11]

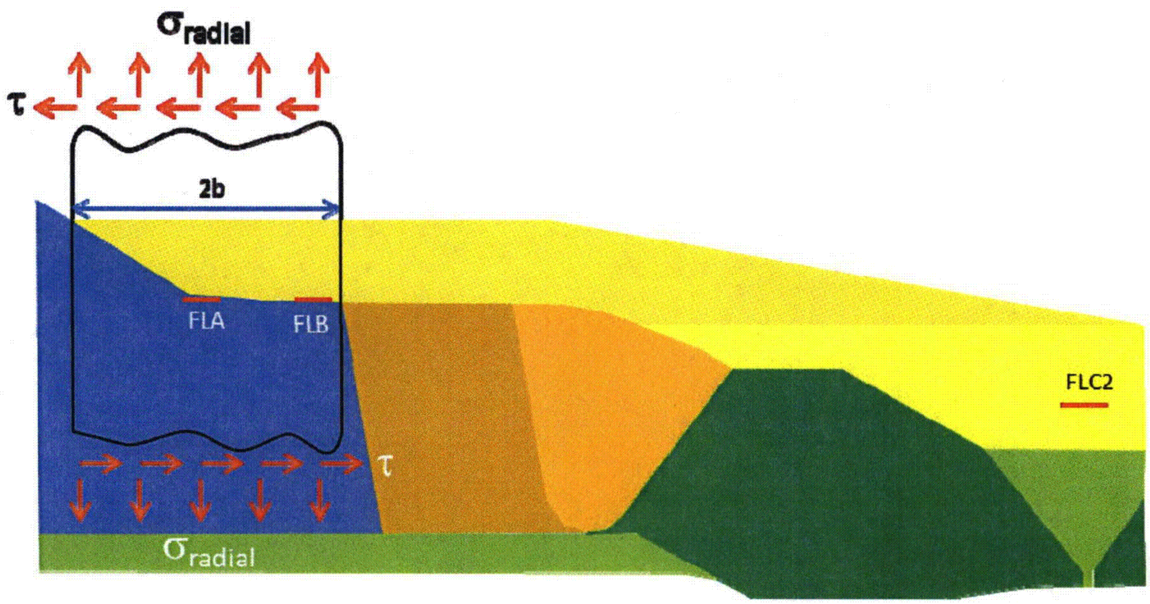


Notes: 1) For laminar indications represented by Flaw FLA (indications - #1, #1A in Nozzle A, Indication #3 in Nozzle C) and FLB (Indication #1, #2 and #3 in Nozzle B) the 2b parameter was defined as the distance between the point where the overlay meets the nozzle on one end and the butter on the other end. This distance is estimated as 1.31".

2) For laminar indication represented by Flaw FLC2 (indication #4 in Nozzle C) the 2b parameter was derived from design drawing minimum overlay conditions Reference [11]

[ ]

**Figure 4-9: Idealization of the Safety Nozzle Laminar Indications**

Figure 4-9 shows idealization of the CCP Model to be used for the Safety nozzle laminar indications. The parameter 2b for FLA is shown for demonstration. The flaw dimensions and the 2b dimensions used for the laminar flaw SIF calculations are listed in Table 4-1.

### 4.2 Material

Reference [12] provides the material designations of various safety nozzle components. The materials related to the laminar flaw path line cases investigated in this document are listed in Table 4-2.

**Table 4-2: Table of Materials**

| Location | Material | Path Line Case |
|---|---|---|
| [ ] | [ ] | [ ] |
| [ ] | [ ] | [ ] |

### 4.3 External Loads

For the PZR Safety Nozzle, the external piping loads applied at the safe end (Table 4-3) can be transferred to the nozzle by the moment arm of 4.09" [11].

**Table 4-3: PZR Safety Nozzle Sustained Loading Conditions at Safe End [5]**

| Load Case | Forces (lbf) | | | Moments (in-lbf) | | |
|---|---|---|---|---|---|---|
| | Axial | $F_y$ | $F_z$ | Torsion | $M_y$ | $M_z$ |
| DW | [ ] | [ ] | [ ] | [ ] | [ ] | [ ] |
| Thermal | [ ] | [ ] | [ ] | [ ] | [ ] | [ ] |
| DE (also known as OBE (±)) | [ ] | [ ] | [ ] | [ ] | [ ] | [ ] |
| DDE | [ ] | [ ] | [ ] | [ ] | [ ] | [ ] |
| HOSGRI | [ ] | [ ] | [ ] | [ ] | [ ] | [ ] |

### 4.4 Operating Stresses

The final flaw sizes are calculated using the same operating transients considered in the original 2007 flaw growth analysis [7]. Per Reference [13], the number of RCS design transients is established for 60 years of design life. The operating transients applicable to laminar flaw growth are listed in Table 4-4.

**Table 4-4: Operating Transients for PZR Safety/Relief Nozzle [7]**

| Transient Number | Designation | Transient Name | Design Cycles |
|---|---|---|---|
| 1 | [ ] | [ ] | [ ] |
| 2 | [ ] | [ ] | [ ] |
| 3 | [ ] | [ ] | [ ] |
| 4 | [ ] | [ ] | [ ] |
| 5 | [ ] | [ ] | [ ] |
| 6 | [ ] | [ ] | [ ] |
| 7 | [ ] | [ ] | [ ] |
| 8 | [ ] | [ ] | [ ] |
| 9 | [ ] | [ ] | [ ] |
| 10 | [ ] | [ ] | [ ] |
| 11 | [ ] | [ ] | [ ] |

(1) Leak Test is included in HUCD Transient.

(2) The Safety Valve Opening transient is conservatively used to also cover the Relief Valve Opening Transient.

(3) An additional transient event due to seismic (OBE) loads is also included for the circumferential flaw analysis. (Note that seismic loading is not expected to contribute to the radial and shear stress components, which constitute the crack driving force for laminar flaw. Thus seismic loading is not considered for fatigue crack growth of laminar flaws) The seismic stress conditions are taken to be the stresses of the steady state condition plus / minus the stresses due to OBE loads shown in Table 4-3.

The cyclic operating stresses that are needed to calculate fatigue crack growth were obtained from a thermo elastic three-dimensional finite element analysis [12]. These fatigue stresses were developed for each of the transients at a number of time points to capture the maximum and minimum stresses due to fluctuations in pressure and temperature. The stresses that are required for crack growth analysis for the flaws are documented in Appendix C of Reference [12]. Radial stresses contributing to Mode I crack growth are from files "SX". Shear stresses contributing to Mode II crack growth are from files "Sh". Since the SIF solutions in Section 2.1.1 are based on uniform stress, the stress data from Appendix C of Reference [12] were sorted to obtain maximum and minimum stresses along the path. These maximum and minimum stresses are conservatively used as the stress values for SIF calculation. In addition, the stress data were further sorted based on time points in each transient. The maximum and minimum radial and shear stresses for all time points in each transient for the path line cases investigated are tabulated in Table 4-5 through Table 4-6.

**Table 4-5: Maximum and Minimum Radial and Shear Stresses on Path Cases FLA_wol and FLA_noz**

| Transient | Path Case FLA_wol | | | | Path Case FLA_noz | | | |
|---|---|---|---|---|---|---|---|---|
| | Minimum Radial Stress $\sigma_{min}$ (ksi) | Maximum Radial Stress $\sigma_{max}$ (ksi) | Minimum Shear Stress $\tau_{min}$ (ksi) | Maximum Shear Stress (ksi) | Minimum Radial Stress $\sigma_{min}$ (ksi) | Maximum Radial Stress $\sigma_{max}$ (ksi) | Minimum Shear Stress $\tau_{min}$ (ksi) | Maximum Shear Stress (ksi) |

*Stresses are due to transient thermal and pressure loads. No residual stress is present in these stresses. These stresses are the minimum and maximum stresses along each pathline for all time points within each transient*

**Table 4-6: Maximum and Minimum Radial and Shear Stresses on Path Cases FLB_wol and FLB_noz**

| Transient | Path Case FLB_wol | | | | Path Case FLB_noz | | | |
|---|---|---|---|---|---|---|---|---|
| | Minimum Radial Stress $\sigma_{min}$ (ksi) | Maximum Radial Stress $\sigma_{max}$ (ksi) | Minimum Shear Stress $\tau_{min}$ (ksi) | Maximum Shear Stress $\tau_{max}$ (ksi) | Minimum Radial Stress $\sigma_{min}$ (ksi) | Maximum Radial Stress $\sigma_{max}$ (ksi) | Minimum Shear Stress $\tau_{min}$ (ksi) | Maximum Shear Stress $\tau_{max}$ (ksi) |

*Stresses are due to transient thermal and pressure loads. No residual stress is present in these stresses. These stresses are the minimum and maximum stresses along each pathline for all time points within each transient*

**Table 4-7: Maximum and Minimum Radial and Shear Stresses on Path Cases FLC2_wol**

| Transient | Path Case FLC2_wol | | | |
|---|---|---|---|---|
| | Minimum Radial Stress $\sigma_{min}$ (ksi) | Maximum Radial Stress $\sigma_{max}$ (ksi) | Minimum Shear Stress $\tau_{min}$ (ksi) | Maximum Shear Stress $\tau_{max}$ (ksi) |

[ ]

*Stresses are due to transient thermal and pressure loads. No residual stress is present in these stresses. These stresses are the minimum and maximum stresses along each pathline for all time points within each transient*

### 4.5 Operating Temperatures

Metal temperature data are required for crack growth calculations. Metal temperatures along path lines were extracted in Appendix C of Reference [12] with file names "TH". The path line temperature data are sorted in the current calculation to determine the maximum temperature along the path from all time points in each transient. The maximum temperatures are used in the fatigue crack growth calculations, which results in a conservative estimate of fatigue crack growth. The maximum temperatures at all path cases during transients are tabulated in Table 4-8.

**Table 4-8: Maximum Temperatures for Path Line Cases**

| Transient | Temperatures for Path Line Cases (°F) | | |
|---|---|---|---|
| | FLA_wol / FLA_noz | FLB_wol / FLB_noz | FLC2_wol |

[ ]

*These temperatures are the maximum temperature along each pathline for a given transient duration.*

### 4.6 Residual Stresses

Residual stresses are analyzed in Reference [14]. The residual stresses at the flaws analyzed in this document are documented in Appendix C of Reference [14]. The maximum values from the bounding cases of radial and shear stresses are tabulated in Table 4-9 and are used for laminar flaw analysis. The axial stresses are tabulated in Table 4-10 and are used for planar circumferential flaw analysis Residual stresses were combined with operating stresses for SIF calculations..

**Table 4-9: Bounding Radial and Shear Weld Residual Stresses for Laminar Flaws**

[

| Location | Radial Stress (ksi) | Shear Stress (ksi) |
|---|---|---|
| | | |
| | | |
| | | |

]

**Table 4-10: Through-Wall Axial Residual Stresses along Path Line "A" for Planar Flaw Evaluation**

[

| Along Path line FLA_pln | |
|---|---|
| Distance Along Path Line from the ID (in.) | Axial WRS (psi) |
| | |

]

## 4.7 Fatigue Crack Growth Laws

Fatigue crack growth models for materials in Table 4-2 are described in the subsections below. Since the flaws in Figure 4-2 and Figure 4-3 do not come in contact with the reactor coolant, crack growth formulae that are applicable in the presence of air environment are used.

### 4.7.1 [ ] - FSWOL

The fatigue crack growth model for Alloy 52 and 52M is obtained from Reference [9], which uses a multiplier of 2 upon those of Alloy 600. The crack growth rate (CGR) equation for Alloy 600 is given in NUREG/CR-6721 [15]. The CGR equation for Alloy 52 and 52M is expressed as,

$$\left(\frac{\mathrm{da}}{\mathrm{dN}}\right)_{\mathrm{A52/52M}} = 2\cdot\left(\frac{\mathrm{da}}{\mathrm{dN}}\right)_{\mathrm{A600}}$$

Substituting the Alloy 600 crack growth equation,

$$\left(\frac{da}{dN}\right)_{A52/52M} = 2\cdot C_{A600} S_R (\Delta K)^n$$

Where ΔK is the stress intensity factor range in terms of MPa√m and da/dN is the crack growth rate in the units of meter/cycle. The other parameters are defined as,

$$C_{A600} = 4.835\times10^{-14} + 1.622\times10^{-16}T - 1.490\times10^{-18}T^2 + 4.355\times10^{-21}T^3$$

$$\Delta K = K_{\max} - K_{\min}$$

$$R = \frac{K_{\min}}{K_{\max}}$$

$$S_R = (1-0.82R)^{-2.2}$$

$$n = 4.1$$

T = metal temperature in °C

For the combined mode loading due to the opening mode (mode I) and sliding mode (mode II) the parameter ΔK was estimated as

$$\Delta K = (\Delta K_I^2 + \Delta K_{II}^2)^{0.5}$$

with $\Delta K_I$ and $\Delta K_{II}$ defined as.

$$\Delta K_I = K_{Imax} - K_{Imin}$$

$$\Delta K_{II} = K_{IImax} - K_{IImin}$$

Where $K_{Imax}$ and $K_{Imin}$ are the maximum and minimum mode I stress intensity factors, and $K_{IImax}$ and $K_{IImin}$ are the maximum and minimum mode II stress intensity factors.

a conservative estimation of the R ratio is given by

$$R = 1 - \Delta K / K_{max}$$

where $K_{max}$ is estimated as

$$K_{max} = (K_{Imax}^2 + K_{IImax}^2)^{0.5}$$

For the case where the R < 0 (or similarly $K_{min} < 0$), R is set equal to zero and the full range of ΔK is used in the crack growth calculations. This is a conservative assumption since crack closure due to compressive stress field is ignored.

### 4.7.2 Low-Alloy Steel - Nozzle

The fatigue crack growth model for low-alloy steel is obtained from Reference [2] Article A-4300. The CGR equation for low-alloy steel is expressed as,

$$\left(\frac{da}{dN}\right)_{LAS} = C_0(\Delta K)^n$$

Where ΔK is the stress intensity factor range in terms of ksi√in and da/dN is the crack growth rate in the units of inch/cycle. The other parameters are defined as,

$$R = \frac{K_{\min}}{K_{\max}}$$

$$\Delta K_{th} = \begin{cases} 5.0 & \text{for } R < 0 \\ 5.0(1-0.8R) & \text{for } 0 \le R < 1.0 \end{cases}$$

$$\text{For } 0 \le R \le 1, \begin{cases} S = 25.72(2.88-R)^{-3.07} \\ \Delta K = K_{\max} - K_{\min} \end{cases}$$

$$\text{For } R_{ratio} < 0, \begin{cases} S = 1 \\ \Delta K = K_{\max} - K_{\min} \end{cases}$$

$$C_0 = \begin{cases} 0 & \text{for } \Delta K < \Delta K_{th} \\ 1.99 \times 10^{-10} S & \text{for } \Delta K \ge \Delta K_{th} \end{cases}$$

$$n = 3.07$$

For the combined mode loading due to the opening mode (mode I) and sliding mode (mode II) the parameter ΔK was estimated as

$$\Delta K = (\Delta K_I^2 + \Delta K_{II}^2)^{0.5}$$

with $\Delta K_I$ and $\Delta K_{II}$ defined as.

$$\Delta K_I = K_{Imax} - K_{Imin}$$

$$\Delta K_{II} = K_{IImax} - K_{IImin}$$

Where $K_{Imax}$ and $K_{Imin}$ are the maximum and minimum mode I stress intensity factors, and $K_{IImax}$ and $K_{IImin}$ are the maximum and minimum mode II stress intensity factors.

a conservative estimation of the R ratio is given by

$$R = 1 - \Delta K / K_{max}$$

where $K_{max}$ is estimated as

$$K_{max} = (K_{Imax}^2 + K_{IImax}^2)^{0.5}$$

Note that for the case where the R < 0 (or similarly $K_{min}$ < 0), it is assumed that $S$ = 1 and $\Delta K = K_{max} - K_{min}$. This is a conservative assumption since crack closure due to compressive stress field is ignored.

## 5.0 COMPUTER USAGE

### 5.1 Software and Hardware

Mathcad [16] and Excel spreadsheets are used in this calculation. The hardware platform (Service Tag# 5VKW5S1) is Intel® Core™ i7-2640M CPU 2.80 GHz, 8.00 GB RAM. The operating system is Microsoft Windows 7 Enterprise, Copyright © 2009, Service Pack 1.

### 5.2 Computer Files

All computer files are listed in this section. All files are available in AREVA NP Inc. ColdStor storage \\cold\General-Access\32\32-9000000\32-9215965-001\official.

**Table 5-1: Computer Files**

| Name | Size | Date/Time Modified | CRC |
|---|---|---|---|
| CircFlaw_NozzleA.xlsm | 2234552 | Mar 09 2014 00:55:21 | 28298 |
| CircFlaw_NozzleA_K.xlsm | 2494168 | Mar 09 2014 01:05:53 | 48888 |
| CircFlaw_NozzleA_K_faulted.xlsm | 2494106 | Mar 09 2014 01:32:43 | 26776 |
| LaminarFlaws.xlsx | 293044 | Mar 06 2014 09:53:04 | 29698 |
| LaminarFlawsA.xlsx | 293140 | Mar 06 2014 09:52:09 | 51342 |
| Laminar_Flaws.xmcd | 861321 | Mar 06 2014 10:44:32 | 39188 |
| Laminar_Flaws_A.xmcd | 920752 | Mar 07 2014 14:09:08 | 55788 |
| TestCase1.xlsm | 200609 | Jan 12 2014 23:30:43 | 01918 |
| TestCase2.xlsm | 206399 | Jan 12 2014 23:31:07 | 64988 |

## 6.0 CALCULATIONS

The fatigue crack growth analysis methods outlined in Section 2.1.2 were used to calculate the final crack sizes for all cracks at the end of 38 years. A total of four cases (along two path lines) were analyzed in this document. All calculations are performed using Mathcad and Excel spreadsheet, as listed in Table 5-1. This section contains sample calculations illustrating the fatigue crack growth analysis for each of the two materials considered in the current document ([ ] and Low Alloy Steel). In each sample calculation, detailed calculations are shown to illustrate fatigue crack growth increment for one transient. The manual calculations were repeated for all transients (not shown in the document) to assure that the manual calculations confirms the results for the first year as reported in Section 7.0

### 6.1 [ ] – FSWOL

Path line cases FLA_wol, FLB_wol and FLC2_wol are located at Alloy 52M material. Using FLA_wol as an example, for transient #1 at the beginning of the first year,

Given

| | | | | | | |
|---|---|---|---|---|---|---|
| $\sigma_{op\ min}$ | = | [ ] | ksi | (Table 4-5) | | |
| $\sigma_{op\ max}$ | = | [ ] | ksi | (Table 4-5) | | |
| $\tau_{op\_min}^{\dagger}$ | = | [ ] | ksi | (Table 4-5) | | |
| $\tau_{op\_max}^{\dagger}$ | = | [ ] | ksi | (Table 4-5) | | |
| $\sigma_{rs}$ | = | [ ] | ksi | (Table 4-9) | | |
| $\tau_{rs}$ | = | [ ] | ksi | (Table 4-9) | | |

Note$^{\dagger}$: conservatively using the largest magnitude of shear stress, which is from the maximum negative stress.

| | | | | | | |
|---|---|---|---|---|---|---|
| 2a | = | [ ] | inch | (Table 4-1) | | |
| 2b | = | [ ] | inch | (Table 4-1) | | |
| T | = | [ ] | °F | (Table 4-8) | [ ] | °C |
| Number of Cycles 60 years | = | [ ] | cycles | (Table 4-4) | | |
| $\Delta N$ | = | [ ] | cycles/year | | | |
| $\sigma_{min} = \sigma_{op\_min} + \sigma_{rs}$ | = | [ ] | ksi | | [ ] | MPa |
| $\sigma_{max} = \sigma_{op\_max} + \sigma_{rs}$ | = | [ ] | ksi | | [ ] | MPa |
| $\tau_{min} = \tau_{op\_min} + \tau_{rs}$ | = | [ ] | ksi | | [ ] | MPa |
| $\tau_{max} = \tau_{op\_max} + \tau_{rs}$ | = | [ ] | ksi | | [ ] | MPa |
| a/b | = | [ ] | | | | |
| $f(a/b) = (1-0.025(a/b)^2+0.06*(a/b)^4)\sqrt{\sec(\pi a/2b)}$ | = | [ ] | | | | |
| $K_{Imin} = \sigma_{max}\sqrt{(\pi a)}\ f(a/b)$ | = | [ ] | ksi√in | | | |
| $K_{Imax} = \sigma_{min}\sqrt{(\pi a)}\ f(a/b)$ | = | [ ] | ksi√in | | | |
| $K_{IImin} = \tau_{max}\sqrt{(\pi a)}\ f(a/b)$ | = | [ ] | ksi√in | | | |
| $K_{IImax} = \tau_{min}\sqrt{(\pi a)}\ f(a/b)$ | = | [ ] | ksi√in | | | |
| $\Delta K_I = K_{Imax} - K_{Imin}$ | = | [ ] | ksi√in | | | |

| | | | | | | |
|---|---|---|---|---|---|---|
| $\Delta K_{II} = K_{IImax} - K_{IImin}$ | = | [ ] | ksi√in | | | |
| $\Delta K = (\Delta K_I^2 + \Delta K_{II}^2)^{0.5}$ | = | [ ] | ksi√in | = | [ ] | MPa√m |
| $K_{max} = (K_{Imax}^2 + K_{IImax}^2)^{0.5}$ | = | [ ] | ksi√in | | | |
| $R = 1 - \Delta K / K_{max}$ | = | [ ] | | | | |
| $S_R = (1 - 0.82\ R)^{-2.2}$ | = | [ ] | | | | |
| $C_{A600} = 4.835 \times 10^{-14} + 1.622 \times 10^{-16} T - 1.490 \times 10^{-18} * T^2 + 4.355 \times 10^{-21} * T^3$ | = | [ ] | | | | |
| $\Delta a = \Delta N(2\ C_{A600}\ S_R\ \Delta K^{4.1})$ | = | [ ] | m | = | [ ] | in |
| $2a = 2a + 2\ \Delta a$ | = | [ ] | | | | |

The calculated 2a = [ ] inch is the initial 2a for the next transient crack growth calculation. After going through all 10 transients in the first year, the crack grows from [ ] , which confirms the results reported in Table 7-1 for the first year. Then, [ ] is used as the initial crack length for the second year calculation and so on. Thus by repeating the process the final flaw size at the end of 38 years is obtained.

### 6.2 Low-Alloy Steel – Nozzle

Path line case FLA_noz and FLB_noz are located at low-alloy steel material. Using FLA_noz as an example, for transient #1 at the beginning of the first year,

| | | | | |
|---|---|---|---|---|
| $\sigma_{op\ min}$ | = | [ ] | ksi | (Table 4-5) |
| $\sigma_{op\ max}$ | = | [ ] | ksi | (Table 4-5) |
| $\tau_{op\_min}$† | = | [ ] | ksi | (Table 4-5) |
| $\tau_{op\_max}$† | = | [ ] | ksi | (Table 4-5) |
| $\sigma_{rs}$ | = | [ ] | ksi | (Table 4-10) |
| $\tau_{rs}$ | = | [ ] | ksi | (Table 4-10) |

Note†: conservatively using the largest magnitude of shear stress, which is from the maximum negative stress.

| | | | | |
|---|---|---|---|---|
| 2a | = | [ ] | inch | (Table 4-1) |
| 2b | = | [ ] | inch | (Table 4-1) |
| T | = | [ ] | °F | (Table 4-8) |
| Number of Cycles 60 years | = | [ ] | | (Table 4-4) |
| ΔN | = | [ ] | cycles/year | |
| $\sigma_{min} = \sigma_{op\_min} + \sigma_{rs}$ | = | [ ] | ksi | |
| $\sigma_{max} = \sigma_{op\_max} + \sigma_{rs}$ | = | [ ] | ksi | |
| $\tau_{min}$† $= \tau_{op\_min} + \tau_{rs}$ | = | [ ] | ksi | |

| | | | |
|---|---|---|---|
| $\tau_{max}\dagger = \tau_{op\_max} + \tau_{rs}$ | = | [ ] | ksi |
| $a/b$ | = | [ ] | |
| $f(a/b) = (1-0.025(a/b)^2+0.06*(a/b)^4)\sqrt{\sec(\pi a/2b)}$ | = | [ ] | |
| $K_{Imin} = \sigma_{max}\sqrt{(\pi a)}\ f(a/b)$ | = | [ ] | ksi√in |
| $K_{Imax} = \sigma_{min}\sqrt{(\pi a)}\ f(a/b)$ | = | [ ] | ksi√in |
| $K_{IImin} = \tau_{max}\sqrt{(\pi a)}\ f(a/b)$ | = | [ ] | ksi√in |
| $K_{IImax} = \tau_{min}\sqrt{(\pi a)}\ f(a/b)$ | = | [ ] | ksi√in |
| $\Delta K_I = K_{Imax} - K_{Imin}$ | = | [ ] | ksi√in |
| $\Delta K_{II} = K_{IImax} - K_{IImin}$ | = | [ ] | ksi√in |
| $\Delta K = (\Delta K_I^2 + \Delta K_{II}^2)^{0.5}$ | = | [ ] | ksi√in |
| $K_{max} = (K_{Imax}^2 + K_{IImax}^2)^{0.5}$ | = | [ ] | ksi√in |
| $R = 1 - \Delta K / K_{max}$ | = | [ ] | |
| $\Delta K_{th} =$ | = | [ ] | ksi√in |
| S (Section 4.7.2) | = | [ ] | |
| Co (Section 4.7.2) | = | [ ] | |
| $\Delta a = \Delta N(C_O \Delta K^{3.07})$ | = | [ ] | inch |
| $2a = 2a + 2\,\Delta a$ | = | [ ] | inch |

The calculated 2a = [ ] inch is the initial 2a for the next transient crack growth calculation. After going through all 10 transients in the first year, the crack grows from [ ] , which confirms the results obtained in Table 7-2 for the first year. Then, [ ] is used as the initial crack length for the second year calculation and so on. Thus by repeating the process the final flaw size at the end of 38 years is obtained.

## 7.0 RESULTS

### 7.1 Laminar Flaws

#### 7.1.1 Laminar Flaw Fatigue Crack Growth Analysis

The crack sizes during 38 years of plant operations due to fatigue crack growths are presented in Table 7-1 through Table 7-4. The final crack sizes for all cases are summarized in Table 7-5. For the two FLA path cases, the larger crack growth is observed on path case FLA_noz, which grew to [ ] . The cracks cases along the FLB_wol grew to [ ] , whereas FLB_noz did not grow at all. The zero crack growth in FLB_noz is found to be the result of calculated ΔK being smaller than ΔK- threshold for fatigue crack growth in Low Alloy Steel. The flaw considered along FLC2_wol grew to [ ] . These bounding final crack sizes for each case are used for laminar flaw evaluations in Section 7.1.2.

**Table 7-1: Fatigue Crack Growth on Path Case FLA_wol**

| Year | Year Start Crack Size (in.) | Crack Growth (in.) | Year End Crack Size (in.) |
|---|---|---|---|

| Year | Year Start Crack Size (in.) | Crack Growth (in.) | Year End Crack Size (in.) |
|---|---|---|---|

[ ]

**Table 7-2: Fatigue Crack Growth on Path Case FLA_noz**

| Year | Year Start Crack Size (in.) | Crack Growth (in.) | Year End Crack Size (in.) |
|---|---|---|---|

[ ]

| Year | Year Start Crack Size (in.) | Crack Growth (in.) | Year End Crack Size (in.) |
|---|---|---|---|

[ ]

Table 7-3: Fatigue Crack Growth on Path Case FLB_wol

| Year | Year Start Crack Size (in.) | Crack Growth (in.) | Year End Crack Size (in.) |
|---|---|---|---|

[ ]

| Year | Year Start Crack Size (in.) | Crack Growth (in.) | Year End Crack Size (in.) |
|---|---|---|---|

**Table 7-4: Fatigue Crack Growth on Path Case FLC2_wol**

| Year | Year Start Crack Size (in.) | Crack Growth (in.) | Year End Crack Size (in.) |
|---|---|---|---|

| Year | Year Start Crack Size (in.) | Crack Growth (in.) | Year End Crack Size (in.) |
|---|---|---|---|

**Table 7-5: Summary of Fatigue Crack Growth Laminar Indications**

| Indication | Path Case | Initial Crack Size (in.) | Final Crack Size (in.) | Crack Increase (%) |
|---|---|---|---|---|

[ ]

### 7.1.2 Laminar Flaw Evaluation

The flaw area calculations are performed in Table 7-6. Based on the areas calculated in Table 7-6, it is concluded that the laminar flaws meet the laminar flaw acceptance criterion in article IWB-3514-3 of ASME Code Section XI [2] after 38 years of plant operation.

The minimum required overlay length evaluation is performed in Table 7-7. It is seen from Table 7-7 that the effective overlay length ($l_{eff}$), evaluated as the actual overlay length ($l_{wol}$) minus the flaw length ($l_{flaw}$), is greater than the minimum required overlay length ($l_{req}$), which is estimated based on Section III of the ASME Code [3]. Thus, it is concluded that the laminar flaws will not impact the overlay integrity after 38 years of plant operation.

**Table 7-6: Flaw Area Evaluation**

| | FLA | FLB | FLC2 | Reference /Comments |
|---|---|---|---|---|
| *Initial flaw width,* $w_{\text{initial}}$ (in.) | [ ] | [ ] | [ ] | Table 7-5 |
| *Final flaw width,* $w_{\text{final}}$ (in.) | [ ] | [ ] | [ ] | Table 7-5 |
| *Initial flaw length,* $l_{\text{initial}}$ (in.) | [ ] | [ ] | [ ] | References [4] and [1] |
| *Final flaw length,* $l_{\text{final}} = (w_{final} / w_{initial})\ l_{initial}$ (in.) | [ ] | [ ] | [ ] | See Note (1) below |
| $A_{cal} = 0.75(w_{final} \times l_{final})$ (in$^2$) | [ ] | [ ] | [ ] | Section 2.1.3 |
| $A_{limit}$ (in$^2$) | 7.5 | 7.5 | 7.5 | Table IWB-3514-3 of [2] |
| Check $A_{cal} \leq A_{limit}$ | OK | OK | OK | |

Note (1): Geometric similar flaw growth is assumed in the growth analysis. This assumption maintains a constant aspect ratio as defined by the initial flaw, $w_{initial}/l_{initial}$. The final flaw length, $l_{final}$ was computed based on $w_{final}$ determined in the growth analysis. The assumption of geometric flaw shape in the growth analysis is conservative since the cyclic stresses acting at the flaw plane are taken as uniform stress over the flaw area. Under uniform stress conditions, the flaw aspect ratio will decrease during growth making the $l_{final}$ smaller than that computed by the constant aspect ratio assumption.

**Table 7-7: Overlay Length Evaluation**

| Parameter | FLA | FLB | FLC2 | Reference/Comments |
|---|---|---|---|---|
| t (in) | [ ] | [ ] | [ ] | Reference [11] |
| OD (in) | [ ] | [ ] | [ ] | Reference [11] |
| $Z_{net}$ ($in^3$) | [ ] | [ ] | [ ] | Equation (2) of Reference [4] |
| $A_{net}$ ($in^2$) | [ ] | [ ] | [ ] | Equation (1) of Reference [4] |
| M (in-lbf) | [ ] | [ ] | [ ] | Faulted, Reference [17] |
| $M/Z_{net}$ (psi) | [ ] | [ ] | [ ] | |
| F (lbf) | [ ] | [ ] | [ ] | Faulted, Reference [17] |
| $F/A_{net}$ (psi) | [ ] | [ ] | [ ] | |
| $M/Z_{net} + F/A_{net}$ (ksi) | [ ] | [ ] | [ ] | Equation (3) of Reference [4] |
| $S_m$ (ksi) | [ ] | [ ] | [ ] | Table 4-2 of Reference [4] |
| $l_{req}$ (in) | [ ] | [ ] | [ ] | Equation (5) of Reference [4] |
| $l_{wol}$ (in) | [ ] | [ ] | [ ] | |
| $l_{flaw}$ (in) | [ ] | [ ] | [ ] | Table 7-5 |
| $l_{eff}$ (in) | [ ] | [ ] | [ ] | Equation (6) of Reference [4] |
| Check $l_{eff} > l_{req}$ | OK | OK | OK | |

Note (1): From Reference [11] [ ]

## 7.2 Planar Indications

### 7.2.1 Nozzle A Circumferential Flaw Fatigue Crack Growth Analysis

The calculated flaw growth for PZR Safety Nozzle A indications was negligible. Table 7-8 shows a summary of the predicted crack growth as calculated by AREVACGC. Table 7-9 shows the contribution of each analyzed transient to the calculated fatigue crack growth.

**Table 7-8: Nozzle A Circumferential Flaw Growth – Summary**

| | |
|---|---|
| Initial Flaw Width, $2a_i$ (in) = | [ ] |
| Initial Flaw Center (in) = | [ ] |
| Final Flaw Width, $2a_f$ (in) = | [ ] |
| Final Flaw Center (in) = | [ ] |
| Growth towards Center (in) = | [ ] |
| Growth away from Center (in) = | [ ] |
| Total Amount of Fatigue Crack Growth (in) = | [ ] |

**Table 7-9: Nozzle A Circumferential Flaw Growth – Detailed Analysis**

| Trans. | Growth (in) | Percent |
|---|---|---|
| HUCD | [ ] | [ ] |
| LDLI | [ ] | [ ] |
| LLD | [ ] | [ ] |
| LOL | [ ] | [ ] |
| LOP | [ ] | [ ] |
| LOF | [ ] | [ ] |
| RT | [ ] | [ ] |
| TRT | [ ] | [ ] |
| IASA | [ ] | [ ] |
| SVO | [ ] | [ ] |
| SEISMIC | [ ] | [ ] |

### 7.2.2 Nozzle A Circumferential Final Flaw Evaluation

As seen in Section 7.2.1, flaw growth is negligible. Table 7-10 shows evaluation of the final flaw depth with flaw acceptance standard from Appendix C of the ASME B&PV Code Section XI [2]. It is seen from Table 7-10 that the final flaw size is much smaller than the allowable flaw size. Therefore, the indications found in PZR Safety Nozzle A are acceptable for the remainder of the plants service life.

**Table 7-10: Nozzle A Circumferential Final Flaw Size Evaluation**

| Allowable Flaw Depths | Normal | Upset | Faulted | Reference |
|---|---|---|---|---|
| Service level maximum pressure, p, (psi) | [ ] | [ ] | [ ] | [7] |
| Service level maximum temperature, T, (F) | [ ] | [ ] | [ ] | [7] |
| Service level flow stress, $\sigma_f$ = (Sy+Su)/2, (psi) | [ ] | [ ] | [ ] | [5] |
| total thickness, t , (inch) | [ ] | [ ] | [ ] | [7] |
| overlay outside diameter, $D_o$, (inch) | [ ] | [ ] | [ ] | [7] |
| sectional area, A, (inch$^2$) | [ ] | [ ] | [ ] | |
| moment of inertia, I, (inch$^4$) | [ ] | [ ] | [ ] | |
| section modulus, S (inch3) | [ ] | [ ] | [ ] | |
| Primary Bending Moment, $M_{b\ SRSS}$ (in-lbf) | [ ] | [ ] | [ ] | See Note 1 below |
| Thermal Expansion Bending Moment, $M_{e\ SRSS}$ (in-lbf) | [ ] | [ ] | [ ] | See Note 1 below |
| Safety factor, SFm, | [ ] | [ ] | [ ] | Ref. [2], C-2621 |
| Safety factor, SFb, | [ ] | [ ] | [ ] | Ref. [2], C-2621 |
| Calculated primary membrane stress, $\sigma_m$ = $pD_o/4t$ , (psi) | [ ] | [ ] | [ ] | Ref. [2], C-2500 |
| Calculated primary bending stress, $\sigma_b$ = Moment SRSS/S , (psi) | [ ] | [ ] | [ ] | Ref. [2], C-2500 |
| Calculated secondary bending stress, $\sigma_e$ = Moment SRSS/S, (psi) | [ ] | [ ] | [ ] | Ref. [2], C-2500 |
| Final Flaw Depth, $a_f$, (in) | [ ] | [ ] | [ ] | |
| Final Flaw length, $l_f$, (in) | [ ] | [ ] | [ ] | |
| Calculated final flaw depth to thickness ratio, $a_f$ /t, | [ ] | [ ] | [ ] | |
| Stress ratio, [$\sigma_m$ + $\sigma_b$ ] / $\sigma_f$ | [ ] | [ ] | [ ] | Ref. [2], Table C-5310-1,2,4 |
| Ratio of flaw length to pipe circumference, $l_f / \pi D_o$, | [ ] | [ ] | [ ] | |
| Ratio of allowable flaw depth to thickness, $a_{allow}$ / t, | 0.750 | 0.750 | 0.750 | Ref. [2], Table C-5310-1,2,4 |

Note: 1) Calculated by transferring the forces and moments in Table 4-3 to the nozzle as indicated in Sec 4.3 and then using the relation described in Section 2.2.3.

The final flaw is also evaluated as if one of its tips is in the ferritic nozzle. The acceptance of the final flaw size was evaluated per the acceptance criteria of IWB-3612. The evaluation is shown in Table 7-11. The controlling normal/upset condition is found to be Loss of Load (LOL) with a maximum applied stress intensity factor of [ ] at a temperature not less than [ ]. The faulted condition stress intensity factor is calculated by adding the stresses due to the faulted condition load as described in Section 2.2.3 to the steady state operating condition stresses. The stress distribution through the thickness is used in calculating the stress intensity factor. For faulted conditions, the maximum stress intensity factor was calculated to be [ ] ksi√in.

Per Article A-4200 of Reference [2], the initiation fracture toughness ($K_{IC}$) and the arrest fracture toughness ($K_{Ia}$) are defined as

$$K_{IC} = 33.2 + 20.734 \exp[0.02(T-RT_{NDT})]$$

$$K_{Ia} = 26.8 + 12.445 \exp[0.0145(T-RT_{NDT})]$$

Where T is the crack tip temperature and $RT_{NDT}$ is the nil-ductility transition temperature. A cut off value of 200 ksi√in upper shelf fracture toughness is imposed on both of the above equations. For the Safety nozzle material an $RT_{NDT}$ value of 60 °F was used. This is a reasonable value for non-irradiated locations such as the location of the Safety nozzle. The value of $K_{IC}$ > 200 ksi√in for T- $RT_{NDT}$ > 105 °F and the value of $K_{Ia}$ > 200 ksi√in for T- $RT_{NDT}$ > 182 °F.

**Table 7-11: Nozzle A Circumferential Final Flaw Margin Evaluation in Ferritic Nozzle**

| Limiting Transient Conditions | Normal/ Upset (LOL) | Faulted | Reference |
|---|---|---|---|
| Limiting Temperature (°F) | [ ] | [ ] | |
| Maximum Stress Intensity Factor (ksi√in) | [ ] | [ ] | Section 5.2: Obtained from AREVACGC output documented in file CircFlaw_NozzleA_K.xlsm |
| Allowed Fracture toughness, $K_{Ia}$ /$K_{IC}$ (ksi√in) | [ ] | [ ] | |
| Obtained Margin | [ ] | [ ] | |
| Required Margin | √10 | √2 | Ref. [2], IWB-3612 |

(1)Since the temperature is above 600°F, using an upper shelf fracture toughness value of 200 ksi√in

The lowest margin obtained for normal/upset conditions is [ ] which is much higher than the required margin of √10. The margin [ ] obtained for faulted condition is also much higher than the required margin of √2. Thus, in both cases the calculated margins are higher than the allowable margins. Therefore, the planar indication found in Safety Nozzle A is acceptable for the remainder of the plants service life.

## 8.0 SUMMARY OF RESULTS

The final crack sizes for all laminar flaw cases are summarized in Table 7-5. The flaw area evaluation and overlay length evaluation are performed in Table 7-6 and Table 7-7, respectively. The final flaw size of the planar flaw is shown in Table 7-8 and the final flaw size evaluation in FSWOL is summarized in Table 7-10. The final flaw size of planar flaw is also evaluated in ferrtic nozzle; the results are shown in Table 7-11.

It is concluded that all the laminar and planar indications found during the inspection of PZR Safety/ Relief Nozzles [1] meet the acceptance criteria of the Section XI of the ASME Code [2] for 38 years of plant operation.

## 9.0 REFERENCES

1. AREVA Document 38-9200149-001, "DCPP Unit 2 Pressurizer Nozzle NDE Data"
2. ASME Boiler and Pressure Vessel Code, Section XI, 2004 Edition with Addenda through 2005
3. ASME Boiler and Pressure Vessel Code, Section III, 2004 Edition with Addenda through 2005
4. AREVA Document 32-9199937-001, "DCPP Unit 2 - Evaluation of Laminar Indications on Pressurizer Nozzles"
5. AREVA Document 32-9199805-001, "Diablo Canyon Power Plant Unit 2 PZR Safety and Spray Nozzles Planar Flaw Analysis"
6. "Safety Evaluation by the Office of Nuclear Reactor Regulation – Request for Relief from the American Society of Mechanical Engineers Boiler and Pressure Vessel Code, Section XI, Inservice Inspection Program, Pacific Gas and Electric Company, Diablo Canyon Power Plant, Unit No. 2 Docket No. 50- 323" Dated February 6, 2008 (ADAMS No. ML080110001)
7. AREVA Document 32-9049065-001, "Diablo Canyon Unit 2 PZR Safety/Relief Nozzle Weld Overlay Crack Growth Evaluation"
8. Hiroshi Tada, Paul C. Paris, George R. Irwin, "The stress analysis of cracks handbook", 3rd edition, ASME, 2000
9. AREVA Document 32-9055891-006, "Fatigue and PWSCC Crack Growth Evaluation Tool AREVACGC."
10. AREVA Document 32- 9052958-003, "Evaluation of stress intensity factors using the weight function method."
11. AREVA Drawing 02-8019311D-001, "Diablo Canyon Pressurizer Safety/ Relief Nozzle Weld Overlay Design Input"
12. AREVA Document 32-9049114-003, "Diablo Canyon Unit 2 - Pressurizer Safety/Relief Nozzle Weld Overlay Analysis"
13. AREVA Document 38-9046469-002, "DCPP 2 Pressurizer Nozzle Weld Overlay Design Data--Non-proprietary"

14. AREVA Document 32-9049062-004, "Diablo Canyon Unit 2 Pressurizer Safety/Relief Nozzle Weld Overlay Residual Stress Analysis"

15. NUREG/CR-6721, "Effects of Alloy Chemistry, Cold Work, and Water Chemistry on Corrosion Fatigue and Stress Corrosion Cracking of Nickel Alloys and Welds," U.S. Nuclear Regulatory Commission (Argonne National Laboratory), April 2001

16. Mathcad 15.0 Software, Parametric Technology Corporation, 140 Kendrick Street, Needham, MA 02494 USA

17. AREVA Document 32-9043545-001, "Diablo Canyon Unit 2, Pressurizer Safety/Relief Nozzle Weld Overlay Sizing Calculation"